Journal of Hydrology 475 (2012) 365–378

Contents lists available at SciVerse ScienceDirect

Journal of Hydrology

journal homepage: www.elsevier.com/locate/jhydrol

Impacts of climate change on temperature and evaporation from a large reservoir in Australia

Fernanda Helfer *, Charles Lemckert, Hong Zhang

Griffith School of Engineering, Griffith University, Gold Coast, QLD, Australia

ARTICLE INFO

Article history:
Received 25 June 2012
Received in revised form 25 September 2012
Accepted 13 October 2012
Available online 22 October 2012
This manuscript was handled by Konstantine P. Georgakakos, Editor-in-Chief, with the assistance of Aiguo Dai, Associate Editor

Keywords:
Climate change
Evaporation
Reservoirs
Temperature

SUMMARY

Determining evaporation rates is essential for efficient management of reservoirs and water resources, particularly in water-scarce countries such as Australia. Today, it is estimated that open water reservoirs in Australia lose around 40% of their total water storage capacity per year to evaporation. While this loss is of significant concern, the threat of a changing climate has been directing greater focus to how much water will be lost from Australia's reservoirs in the future. This paper analyses evaporation rates from a large water supply reservoir in South-East Queensland (SEQ), Australia, under current climate and predicted climate change conditions using modelling. Daily meteorological projections from nine global climate models were used in the model DYRESM as the driving forces of the thermodynamics of the reservoir under study. Two future 20-year period simulations were undertaken, one from 2030 to 2050, and the other from 2070 to 2090. The modelled future evaporation rates, as well as water temperatures, were then compared with modelled evaporation rates and temperatures obtained using observed meteorological variables for the period of 1990–2010. The results showed that the evaporation rates from the study reservoir will increase in the future. For the period centred in 2040, the annual evaporation will be approximately 8% higher than the 20-year average annual evaporation estimated for the present climate. A more pronounced increase in evaporation is expected in 2070–2090, with annual evaporation predictions being approximately 15% higher than the baseline evaporation. The main agent behind this increase is higher surface air temperatures in the future. According to the modelling results, the mean annual surface air temperature will grow from the present value of 20.4 °C to 21.5 °C in 2030–2050, and to 23.2 °C in 2070–2090. As a consequence, the mean annual surface water temperatures of the reservoir will increase by 0.9 °C and 1.7 °C in both timeframes, respectively. This will have a significant impact on the evaporation rates, particularly in spring and summer, when the temperature increases will be more significant.

1. Introduction

Australia and most semi-arid countries around the world rely on water stored in reservoirs for drinking water supply and food production. However, the rates of evaporation in these countries can be exceedingly large. In Australia, around 40% of its total water storage capacity is lost per year due to high rates of evaporation (Craig et al., 2005). Concerns over Australia's future open water evaporation rates are increasing due to the threat of a changing climate. In fact, there are indications that the meteorological factors involved in the process of evaporation will be significantly affected as a result of increasing greenhouse gas (GHG) emissions. The 2007 Australian Climate Change Report by the Commonwealth Scientific and Industrial Research Organisation (CSIRO) and Bureau of Meteorology (BoM) is probably the best source of information on how the Australian climate will change from now, and into the future (CSIRO and BoM, 2007). This report is based on results from 23 different global climate models used within the Intergovernmental Panel on Climate Change Fourth Assessment Report (IPCC, 2007). Projections for most climatic variables are given for a range of GHG emission scenarios. According to the CSIRO and BoM (2007), there is a growing body of evidence in support of an increase in Australian air temperatures, with an increase of 0.9 °C since 1950. For the future, the estimate of warming by 2030 relative to the base climate of 1990 is approximately 1.0 °C, with warming of around 0.8 °C in coastal areas and 1.1 °C inland. By 2050, warming in Australia will range from 1.2 °C to 2.2 °C for low and high emission scenarios, respectively, and by 2070, from around 1.8 °C to 3.4 °C.

As a result of the change in climate, particularly the increase in surface air temperatures, evaporation is also expected to increase throughout Australia. According to CSIRO and BoM (2007), the largest increases in potential evapotranspiration are expected in the north and east, where the changes by 2030 are estimated to

* Corresponding author. Address: Building G09, Room 1.02, Griffith School of Engineering, Gold Coast Campus, Griffith University, QLD 4222, Australia. Tel.: +61 (0)7 5552 7608; fax: +61 (0)7 5552 8065.
E-mail address: f.helfer@griffith.edu.au (F. Helfer).

0022-1694/$ - see front matter © 2012 Elsevier B.V. All rights reserved.
http://dx.doi.org/10.1016/j.jhydrol.2012.10.008

be around 2%. By 2070, the low emission scenario shows increases in evapotranspiration of around 3% in the south and west, and around 6% in the north and east, while the high emission scenario shows increases of around 6% in the south and west, and 10% in the north and east. Johnson and Sharma (2010) analysed evaporation changes over Australia using outputs from five global climate models and the Penman model for open water evaporation (Brutsaert, 1982). The mean percentage change in open water body evaporation across Australia was found to be 2.2% for 2030, 3.9% for 2050 and 6.8% for 2070 in a high emission scenario, and 1.7%, 3.9%, and 4.8% for 2030, 2050 and 2070, respectively, in a low emission scenario.

Despite this overall picture of future potential evapotranspiration in Australia, the effects of climate change on evaporation from and thermodynamics of particular lakes can only be determined by performing a site-specific investigation. This can be undertaken using site-specific projections for the meteorological variables that drive the evaporation process, namely solar radiation, air temperature, wind speed and vapour pressure. Evaporation under climate change in Australia has only been assessed on a broad scale, based on meteorological projections generated by global climate models. These do not incorporate local climate variations, and therefore are inappropriate for finer scale analyses, such as the study of evaporation from reservoirs. Local studies on evaporation should be based on meteorological data derived specifically for the study site and should incorporate the regional pattern variations of the local climate.

After obtaining the appropriate meteorological data, the study of the response of lakes to climate change can be achieved by using numerical modelling simulation. In the modelling of lakes under climate change conditions, the predicted future thermodynamics and evaporation driving forces are incorporated in the model, and the responses of the lakes to these forces are obtained in a relatively short period of time. This further facilitates the investigation of the behaviour of lakes under different climate change scenarios and allows a portfolio of all possible outcomes to be created.

Daily climate change projections into the current century for any country can be obtained from global climate models, as mentioned earlier. Global climate models, also known as general circulation models (GCMs), are models that solve the primitive equations of mass, momentum and thermodynamics to generate a description of the state of the atmosphere, and produce most of the meteorological variables, such as wind speed, relative humidity, rainfall, surface air temperature and solar radiation. The GCMs are typically used together, as a multi-model analysis, where long time series into the future and different GHG emission scenarios are used in order to create climatic statistics (Nunez and McGregor, 2007). This multi-model approach allows for a first look at the likability of future climate changes, which is usually referred to as climate change ensemble projection or climate change "envelope".

Inherent to GCMs, however, is their coarse spatial resolution which, amongst all the available models, varies from 200 to 500 km. With this resolution, albeit GCMs incorporate the important large-scale atmospheric circulation, they are unable to capture local-scale factors, such as the orographic elevation, proximity to water bodies and local winds. One way to work around this is to downscale the GCM datasets to a regional scale using a regional climate model (RCM) with atmospheric forcings based on the outputs of the GCM. In this way, the local climate trends are captured, while maintaining agreement with the large-scale response of each GCM (Thatcher and McGregor, 2011). For instance, Sahoo and Schladow (2008) used meteorological projections from the global climate model GFDL (Delworth et al., 2006) downscaled to the California-Nevada region to study the impacts of climate change on the dynamics of lakes and reservoirs in that region. Likewise, McGregor and Nguyen (2010) used downscaled projections forced by sea-surface temperatures from the CSIRO-Mk 3.5 model (Gordon et al., 2010) to study the future climate of the Murray-Darling Basin, Australia. Furthermore, Nguyen et al. (2011) utilised the downscaling technique for six global climate models to investigate the local climate of the Pacific island nations. Also, Yilmaz and Imteaz (2011) downscaled data from the GCM ECHAM5 in order to simulate snowmelt runoff from upper Euphrates basin. According to these authors, high-resolution simulations provide a better resolution of spatial details and of extremes, in addition to yielding boundary conditions for even finer resolution simulations.

Kay and Davies (2008), for example, investigated the differences in the estimation of monthly potential evaporation in Britain when using outputs from either GCMs or RCMs. They utilised the Penman–Monteith model and a simple temperature-based model in the estimations of evaporation for the current climate. The results were compared to a gridded dataset derived from a modified Penman–Monteith formulation using meteorological observations. According to their results, RCMs' outputs are able to generate monthly evaporation rates that show much closer agreement with evaporation rates derived from observed data as compared to GCMs' outputs.

In Australia, the CSIRO has converted broad-scale climate change projections from a wide range of GCMs into local-scale regional projections for the South-East Queensland (SEQ) region using the regional climate model CSIRO Conformal-Cubic Atmospheric Model (CCAM) (McGregor, 2005; McGregor and Dix, 2001, 2008). The finer scale detail of these downscaled projections varies from 15 km to 60 km and thus they are more reflective of regional considerations than the popular GCM outputs, and thereby more representative of a plausible future.

In this context, the aim of this paper was to investigate the influences of a changing climate on evaporation from a large and important water body located in SEQ, Australia. Meteorological projections from nine GCMs, subsequent to the CCAM dynamical downscaling, were used in a validated dynamic reservoir model (Helfer et al., 2011). Modelled future volume-averaged lake temperatures, lake surface temperatures and evaporation rates were analysed and compared with the present-day modelled temperatures and evaporation rates. Also, causes and implications of lake temperature and evaporation changes are briefly discussed. The outcomes of this research provide a first indication of the most likely changes in evaporation and water temperatures expected for reservoirs in the SEQ region for all seasons, as well as a better understanding of the drivers of these changes. This study also provides a warning of the possible changes for which the region should be prepared in terms of water availability in the future.

2. Study site and meteorological data for simulations

For this study, a large reservoir located in SEQ was considered. Wivenhoe Dam (27°23′11″S, 152°37′10″E, Fig. 1) is built on the Brisbane River and is located approximately 40 km northwest of Brisbane. Its main purposes are flood mitigation and the supply of potable water to the SEQ region. At full capacity, this dam has a volume of 1160 hm^3 and a surface area of 107 km^2, with a maximum depth of 40 m.

The meteorological data for the nearest official weather station, located 25 km from Wivenhoe Dam, was provided by the BoM. This was the nearest station with a considerably long, reliable and consistent set of historical meteorological data. Daily data from 01/01/1990 to 31/12/2010 were used in the simulations to compose the baseline (or present-day) scenario. This long-term set of data allowed for an accurate estimation of the present-day average thermal behaviour and evaporation of the reservoir.

Future daily projections for solar radiation, wind speed, air temperature, air humidity and rainfall over the SEQ region were provided by the CSIRO. Although there are currently 23 GCMs

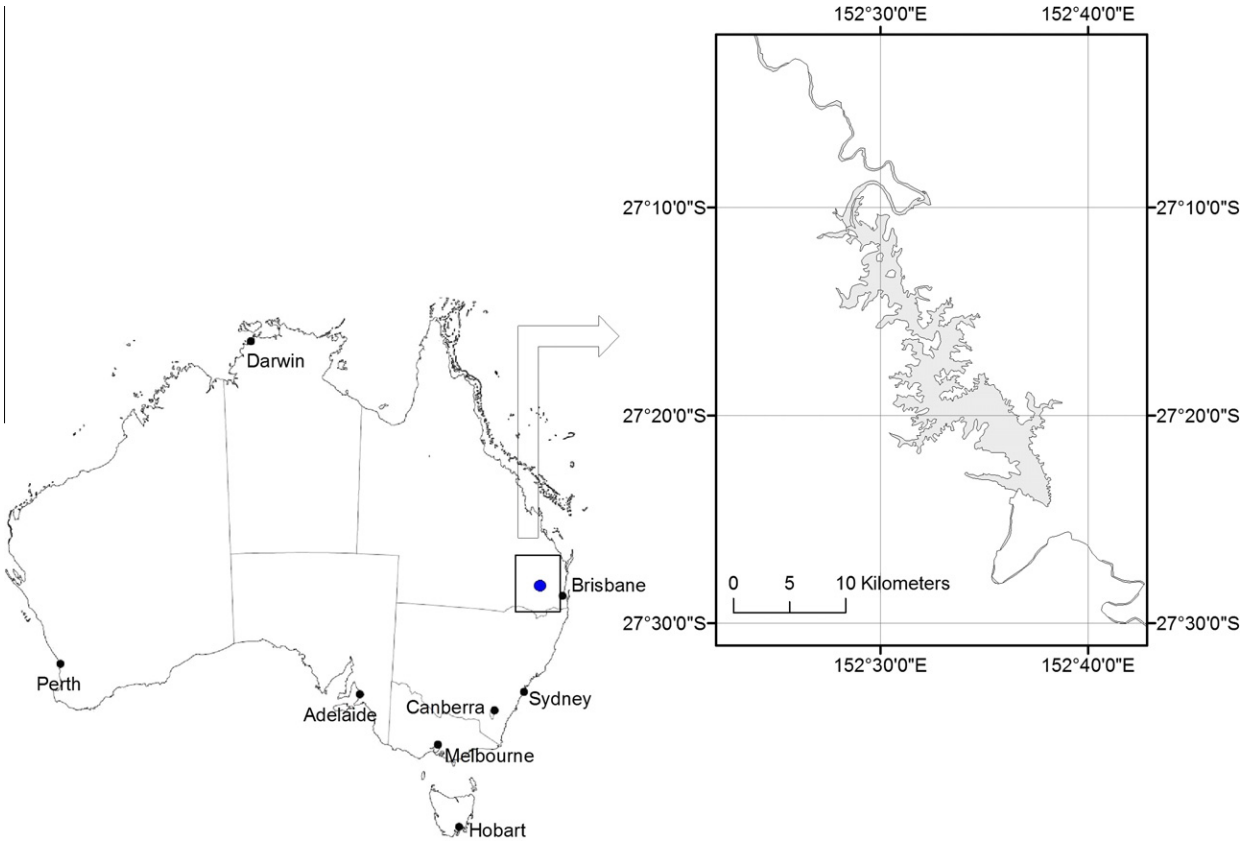

Fig. 1. Location of Wivenhoe Dam (shaded area) in Australia (modified from Helfer et al., 2011).

available from the World Climate Research Programme (WCRP) Coupled Model Intercomparison Project phase 3 (CMIP3) multi-model dataset archive (Meehl et al., 2007), only nine GCMs were considered by CSIRO for downscaling in SEQ (Table 1). The selection of these GCMs was predicated on the models' efficacy in predicting the present-day climate, particularly the seasonal variability, throughout Australia. The nine host GCMs were used to derive daily data on a 15-km resolution grid over the SEQ region using dynamical downscaling with the Conformal-Cubic Atmospheric Model (CCAM). The downscaling technique is described in Nguyen et al. (2011). Meteorological data at the location 27°22′12″S, 152°36′00″E was extracted from the grid. This point coincides with the centre of the southern portion of the dam, where the greatest depth occurs.

The efficacy of climate models in simulating the current climate has been represented in literature by different skill scores. Perhaps one of the most reasonable ranking systems available for daily projections is the one proposed by Perkins et al. (2007). These authors ranked all the available GCMs based on how well each model represents the observed probability density functions of daily precipitation and maximum and minimum surface air temperatures in Australia. Watterson (1996), on the other hand, ranked a larger range of GCMs based on the agreement between modelled and observed seasonal-mean temperature, precipitation and sea level pressure in Australia. In this system, a single 4 value between 1 (perfect match) and 0 (no-skill) is obtained for each model, variable and season, based on pattern correlations and root-mean-square errors. It is on the *M* score, rather than on the score by Perkins et al. (2007) that the choice of the GCMs utilised in this study was based. This is due to a larger range of models covered by this system. The *M* value of each model is presented in Table 1. The value represents the mean skill score for each of the three aforementioned meteorological variables for each of the four seasons (that is, a mean of a total of 12 scores). The mean skill scores of the selected models are all above 0.6, meaning that they have high ability to predict the Australian climate. In this study, a method of weighting the models' performance based on the *M* scores, as a means to obtain a clearer sign of the likely change (Kirono and Kent, 2011) was also considered, as described in Section 5.

2.1. Bias correction

In this section, the approach to remove the biases (errors) from the projections derived from the nine models used in this study is described. The bias correction method is based on the delta change approach, a method that has been extensively discussed and applied in similar studies based on climate model predictions (e.g., Hay et al., 2000; Lenderink et al., 2007; van Roosmalen et al., 2010; Xu and Zong-Liang, 2012).

As described earlier, the time period from 01/01/1990 to 31/12/2010 was adopted as the baseline (or present-day) scenario in this study. Observed daily meteorological variables (precipitation, air temperature, solar radiation, wind speed and relative humidity) for this period were first compared against the meteorological variables derived from the nine climate models for the same period. Even though all models reproduced the seasonal cycle of the five meteorological variables quite well (particularly surface air temperature, solar radiation and humidity), almost all of the models showed significant discrepancies at some time for some particular months and for some variables, in comparison to the observed data. For example, in general, all models underestimated solar radiation and air temperature in all months. Also, the models significantly overestimated precipitation, particularly between March and August. They also overestimated wind speed in spring. As for

Table 1
List of the climate models adopted in this study.

Model name[a]	Centre	Country	Original Resolution (lat × long)	Key reference	*M* skill score
CSIRO-Mk3.0	CSIRO atmospheric research	Australia	~1.80° × 1.80°	Gordon et al. (2002)	0.601
CSIRO-Mk3.5	CSIRO atmospheric research	Australia	~1.80° × 1.80°	Gordon et al. (2010)	0.607
ECHAM5/MPI-OM	Max planck institute for meteorology	Germany	~1.80° × 1.80°	Roeckner et al. (2003)	0.700
GFDL-CM2.1	US Dept. of commerce/NOAA/geophysical fluid dynamics laboratory	USA	~2.0° × 2.5°	Delworth et al. (2006)	0.672
INM-CM3.0	Institute for numerical mathematics	Russia	~4.0° × 5.0°	Diansky and Volodin (2002)	0.627
MIROC3.2 (medres)	Center for climate system research (the university of tokyo), national institute for environmental studies, and frontier research center for global change (JAMSTEC)	Japan	~2.8° × 2.8°	Hasumi et al., 2004	0.608
UKMO-HadCM3	Hadley centre for climate prediction and research/met office	UK	~2.5° × 3.75°	Pope et al., 2000; Gordon et al., 2000	0.608
UKMO-HadGEM1	Hadley centre for climate prediction and research/met office	UK	~1.25° × 1.875°	Johns et al. (2006), Martin et al. (2006) and Ringer et al. (2006)	0.674
CCSM3	National center for atmospheric research	USA	~1.4° × 1.4°	Collins et al. (2006)	0.677

[a] Models were downscaled to ~15 km resolution using CCAM.

vapour pressure, there was a generalised underestimation in summer. These biases were removed using the statistical approach described below.

The delta change bias removal approach is a statistical correction method which aims to produce long-term time-series that have a monthly (or seasonal) statistical mean close to that of the observations. The standard delta change method consists of computing long-term averages of monthly (seasonal) differences between the modelled time-series in the control scenario and the modelled time-series in the future scenario. The method assumes that these biases (i.e., the monthly or seasonal differences between present and future modelled data) do not change over time. In order to produce a future time-series of the meteorological variables, these calculated biases are applied to the observed historical climate data. The delta method thus assumes that future model biases for both mean and variability will be the same as those in present-day simulations.

In this study, an adapted approach based on the delta change method was used. In this approach, the biases were calculated for the present-day scenario as being the difference between the modelled and the observed data. These changes were then subtracted from the modelled future daily time-series. More precisely, instead of creating databases for the future by altering an observed current database of meteorological variables with delta change factors, the modelled future daily databases were altered with the delta change factors obtained from the mean difference between present-day modelled and observed time-series. This is justifiable because future data on a daily basis was available for this study. The standard method would be more appropriate in the case where future data is only available on a monthly basis, and there is a need to obtain daily data series for future simulations.

Another innovation of the approach utilised in this study is the use of the running monthly mean value instead of the simple monthly mean in the estimation of the delta change factors. This method was suggested by Haerter et al. (2011) to avoid discontinuities at the interfaces between months. For state variables, such as relative humidity and surface air temperature, the delta changes (Δs) were computed for each day i as:

$$\Delta s(i) = \overline{V_{m,p}}(i) - \overline{V_{o,p}}(i); \quad i = 1, 2, \ldots, 365 \tag{1}$$

where the indices 'm' and 'o' stand for modelled and observed data respectively, and the index 'p' refers to the reference period (1991–2010). $\overline{V}(i)$ is the running 31-day mean value for all 20 years of the reference period, and involves the previous and subsequent 15 days to avoid discontinuities at the interfaces between calendar months, and is given as:

$$\overline{V}(i) = \begin{cases} \frac{1}{31}\sum_{j=i-15}^{i+15} V(j); & 15 < i \leqslant 350 \\ \frac{1}{31}\left(\sum_{j=1}^{i+15} V(j) + \sum_{j=365-(15-i)}^{365} V(j)\right); & 1 \leqslant i \leqslant 15 \\ \frac{1}{31}\left(\sum_{j=i-15}^{365} V(j) + \sum_{j=1}^{15-(365-i)} V(j)\right); & 350 < i \leqslant 365 \end{cases} \tag{2}$$

For flux variables, such as solar radiation, wind speed and precipitation, the delta changes (Δf) were computed for each day as:

$$\Delta f(i) = \frac{\overline{V_{o,p}}(i)}{\overline{V_{m,p}}(i)}; \quad i = 1, 2, \ldots, 365 \tag{3}$$

For leap years, an additional delta change factor was used after day 59. The value of this factor was considered as the same as the one calculated for day 59.

To remove the biases from the future modelled time-series, the following procedures were used. For relative humidity and air temperature, the new databases were generated as:

$$V_{c,f}(i) = V_{m,f}(i) - \Delta s(i); \quad i = 1, 2, \ldots, 365 \tag{4}$$

where $V_{c,f}(i)$ represents each daily value in the future corrected databases and $V_{m,f}(i)$ is the original modelled daily value in the uncorrected databases. For solar radiation, wind speed and precipitation, the procedure was:

$$V_{c,f}(i) = V_{m,f}(i)\Delta f(i); \quad i = 1, 2, \ldots, 365 \tag{5}$$

The method of bias correction was tested with the observed and modelled daily data series for the reference time period (1991–2010). The method significantly improved the data series, as shown in Fig. 2. For instance, the mean biases in monthly solar radiation were reduced from −3.3% to −0.09%. Vapour pressure mean biases decreased from −4.3% to −0.09%. For monthly wind speed, the errors were reduced from 3.8% to −0.04%. The mean biases in air temperature were reduced from −6% to −0.02%, and in rainfall, from 40% to 0.3%.

3. Simulations

All simulations to estimate Wivenhoe Dam's temperatures and evaporation rates were performed with the 1-D model DYRESM. This hydrodynamic model simulates lake thermodynamic processes and lake surface mass fluxes using meteorological variables, inflows and outflows as driving forces. The model is described in brief in the following section.

For the present-day simulation, daily observed meteorological variables from 1990 to 2010 were used in the model. For the future simulations, two distinct 20-year periods were chosen, one around 2040 and one around 2080. The daily future meteorological projections were obtained from 9 climate models and passed through a bias correction algorithm to reduce systematic errors, as described in the previous section.

The future scenarios were simulated in the SRES-A2 emission scenario (IPCC, 2000). The SRES-A2 scenario comprises a high GHG emission scenario in which the concentration of CO_2 reaches 850 ppmv (parts per million by volume) by 2100. As current emission levels are at, or are already above those specified for this scenario (Raupach et al., 2007), the SRES-A2 scenario appeared to be the most realistic choice. Other similar studies, such as Kay et al. (2006), Charles et al. (2007), Kay and Davies (2008), Leander et al. (2008), Chu et al. (2010), Nguyen et al. (2011) and Yilmaz and Imteaz (2011) have also opted for this scenario.

The initial depth of Wivenhoe Dam was set at full capacity (40 m) and water column temperatures were assumed to be the same temperatures as measured in January 2007. The very high similarity between the air temperatures in 2007 and 1990 was the main reason for this approach, which implies that the lake had similar water temperatures in January for those two years. As these values only approximate actual initial conditions, a model warm-up period was considered. Previous sensitivity tests have indicated that Wivenhoe Dam reaches equilibrium with external forcings within one month (Helfer et al., 2011).

Also for the simulations, vertical mixing processes were assumed to be more important than horizontal advective processes, such as inflows and outflows, in determining the vertical temperature distribution in the study reservoir. In large reservoirs, such as Wivenhoe Dam, where inflows and outflows have only localized effects on water temperature, these flows may be ignored when predicting the temperature in the central portion of the lake (Ivey and Patterson, 1984). Other studies on the temperature dynamics of Wivenhoe Dam (e.g., Yao, 2008; Helfer et al., 2011) have found close agreement between modelled and measured water temperatures without considering inflows and outflows. Therefore, the only water contribution to the dam was the rainfall, and the outflow was the evaporation.

4. Modelling with DYRESM

In this study, the one-dimensional processed-based model DYRESM was used to model the lake mixing dynamics and to predict water temperatures and evaporation rates from Wivenhoe Dam. The model was previously calibrated for Wivenhoe Dam against measured water temperatures, and the validation for evaporation was based on measured data obtained for a nearby dam. Full details of the validation and calibration of the model are described in Helfer et al. (2011).

An extensive description of DYRESM has been given in literature (e.g., Imberger et al., 1978; Spigel and Imberger, 1980; Imberger and Patterson, 1981; Patterson et al., 1984; Hocking et al., 1988; Patterson and Imberger, 1989). In brief, DYRESM takes daily or sub-daily meteorological forcing data (solar radiation, wind, surface air temperature and air humidity), volume of inflows and outflows, and then produces outputs for water depth, water temperature, salinity and density. The model assumes horizontal homogeneity, which is based on the lake density stratification. Vertical motions are inhibited by this stratification, while horizontal variations in density are quickly relaxed by horizontal advection and convection.

The basic processes modelled by DYRESM are surface heat and mass transfer, dynamics of the surface layer, vertical diffusion in the hypolimnion, and inflow and outflow dynamics. The model makes use of the Lagrangian layer concept in which the lake is represented by a series of horizontal layers, each with uniform properties but variable thickness. These layers are able to expand, contract, amalgamate, subdivide and move up and down as they are affected by the inflows, outflows, evaporation and rainfall.

Within the scope of this paper, the processes which are most important are those controlling the surface layer. The surface heat, mass and momentum exchanges comprise the primary mechanisms for heating, mixing and stratifying a water body in DYRESM. The surface layer dynamics is based on an integral turbulent kinetic energy model (Sherman et al., 1978; Yeates and Imberger, 2003). The turbulent kinetic energy budget is computed through three main processes: convective overturn (where energy is released from the decrease in potential energy resulting from dense water falling to a lower level), stirring (where energy from the wind stress is applied to the surface layer), and shear (where kinetic energy is transferred from upper to the lower layers in the water column). The total available energy and the required potential energy for mixing the surface mixed layer and the adjacent layer are compared. If the energy available is greater than the energy required for mixing, the mixed layer is deepened and the available energy is decremented by the required energy. The process is repeated until there is no remaining energy to continue the deepening process.

Whenever layers are mixed together, the layer properties are redistributed according to the conservation laws:

$$C_{\text{new}} = \frac{C_i M_i + C_{i+1} M_{i+1}}{M_i + M_{i+1}} \tag{6}$$

where the subscripts refer to layer indices, C is the property being conserved (energy, salt or momentum) and M is the layer mass.

The surface heat fluxes include heating due to shortwave and long-wave radiation, sensible heat and latent heat. The fluxes of long-wave radiation, sensible heat and evaporation are assumed to operate on the surface layer only. Short-wave radiation is

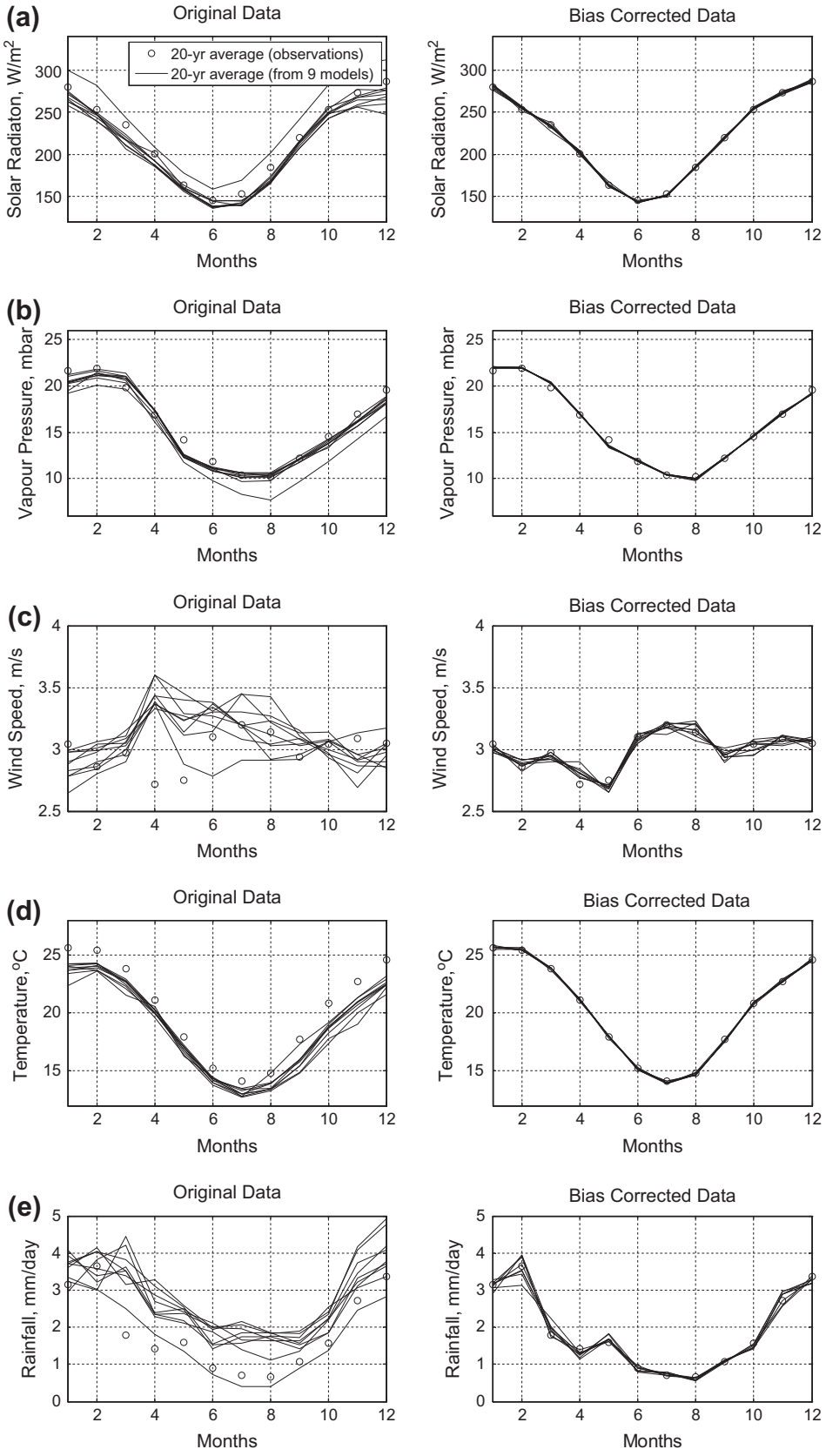

Fig. 2. Long-term monthly averages for solar radiation (a), vapour pressure (b), wind speed (c), temperature (d) and rainfall (e) before and after bias correction. Shown are observations (circles) and simulations from 9 climate models (solid lines), each averaged over 1991–2010.

assumed to act not only on the surface layer, but also in the water column, penetrating the water depth according to the Beer–Lambert law, as a function of the light extinction coefficient. The quantity of radiation reaching the surface of the lake depends on

the albedo of the water. The penetrative radiation is assumed to be 45% of the radiation reaching the surface. Long wave radiation emitted from the lake is calculated according to the Stefan–Boltzmann law, as a function of the emissivity and temperature of the water surface.

The sensible and latent heat fluxes are described by bulk aerodynamic formulae (Brutsaert, 1982). For the evaporative heat flux, which is most important for the present discussion, the bulk aerodynamic formula is given as:

$$Q_E = \rho_a \lambda C_E U(q_a - q_s) \quad (7)$$

where Q_E is the latent heat flux due to evaporation (W m^{-2}), ρ_a is the air density, λ is the latent heat of evaporation, C_E is the latent heat transfer coefficient, U is the wind speed at the reference height of 10 m, q_a is the specific humidity in the air and q_s is the specific humidity at saturation pressure, which is a function of the surface water temperature.

The surface mass exchanges include mass input from precipitation and output from evaporation. The mass of the evaporated water is calculated as:

$$M_N = -\frac{Q_E A_N}{\lambda} \quad (8)$$

where M_N is the evaporating mass from the surface layer with area A_N. The total change in water mass in the surface layer in each time interval is given by the difference between the rainfall and the evaporation.

5. Results and discussion

5.1. Present-day scenario (1991–2010)

This section describes the average climate of the baseline scenario, giving emphasis to the driving forces of evaporation (surface air temperature, solar radiation, humidity and wind speed). The results of modelled lake temperature and evaporation in the present-day scenario are then discussed. Being the model warm-up period, the year of 1990 is not included in these analyses.

Fig. 3 presents the seasonal variability in surface air temperature, wind speed, solar radiation and vapour pressure at Wivenhoe Dam for the 20-year set of data from 1991 to 2010. These variables were selected for presentation due to their relevance in the process of evaporation. The whiskers show the year-to-year variability and range from the 10th to the 90th percentiles of the observations.

As presented in Fig. 3, the Wivenhoe Dam region is characterized by four well-defined seasons, with hot, humid summers and relatively cold, dry winters. The mean annual temperature is around 20 °C, with the air temperature in summer being around 25 °C and in winter, 15 °C. These temperatures characterize a typical temperate climate. Solar radiation at Wivenhoe Dam is also seasonal, with higher values in summer than winter. Similarly, vapour pressure follows the same trend as air temperature and solar radiation, with high values in summer and low values in winter. The deficit of vapour pressure (not shown in Fig. 3) is also higher in summer, indicating that higher rates of evaporation are expected during this season. Wind speed, on the other hand, does not follow a seasonal trend. The average wind speed over the 20-year period was 3 m s^{-1}.

The modelled 20-year average seasonal daily evaporation from Wivenhoe Dam is presented in Fig. 4. There is a clear difference between evaporation in winter and summer. The 20-year average daily evaporation is 3.6 mm. Daily evaporation in summer is around 5 mm, whereas in winter it is around 2 mm. In spring and summer, the daily evaporation is about 3.6 mm. In summer, the 20-year average total evaporation is 450 mm and in winter it is 190 mm. Evaporation in spring and autumn falls between these two extremes, at around 330 mm. The 20-year average evaporation from the dam is 1300 mm, varying from 1080 to 1490 mm.

The modelled temperature of Wivenhoe Dam for the period of simulation is presented in Fig. 5. The variation in water depth over the years has been omitted in the Figure, as this is a free-surface representation of the lake's temperatures. There is a notably consistent pattern in the variation of the lake temperatures, with high temperatures in summer and low temperatures in winter. This pattern is a result of the seasonal variation in the surface air temperatures and solar radiation shown previously in Fig. 3. The 20-year average lake surface temperature is 22.4 °C, with an average of 28.2 °C in summer and 15.6 °C in winter. The lake bottom temperature is nearly constant in Wivenhoe Dam, with an average of 15.2 °C, oscillating between 15.4 °C in summer and 14.8 °C in winter. The 20-year average volume-averaged lake temperature is 19.1 °C, varying from an average of 22.1 °C in summer and 15.3 °C in winter.

Also notable in Fig. 5 is the pattern of thermal stratification in Wivenhoe Dam. Wivenhoe Dam is a warm monomictic lake that stratifies from September until the beginning of May, covering spring, summer and the autumn seasons. During winter, Wivenhoe Dam is characterized by well-mixed water columns due to the lake's turnover. Fig. 6 shows measured in-lake temperature profiles during the year of 2007. Field measurements were obtained from SEQ Water.

Thermal stratification is considered an important regulator of the overall metabolism of a lake. The epilimnion – upper and warm water layer – is usually well mixed as it is subject to mixing induced by the wind. On the other hand, the hypolimnion – bottom layer of colder water – experiences limited mixing because it is isolated from surface energy inputs due to the existence of a thermocline region between itself and the epilimnion. This region, called metalimnion, limits the exchange of dissolved substances between the epilimnion and the hypolimnion due to the lowering of turbulence and mixing. Limited mixing has important implications for the cycling of critical constituents such as nutrients and dissolved oxygen. As shown in Fig. 6, in Wivenhoe Dam, the metalimnion is present during almost the entire yearly cycle, with the highest thermal gradients occurring from November to April. The depth of the epilimnion (or depth of the well mixed layer) is indicative of the level of mixing in the lake. In Wivenhoe Dam, the depth of the mixed layer has an average of 3.6 m in summer, 6.8 m in autumn, 5.0 m in spring and it is well mixed from top to bottom during winter.

5.2. Future scenarios

This section firstly describes the future climate at Wivenhoe Dam, pointing out the main changes in the driving forces of evaporation – namely air temperature, wind speed, solar radiation and air vapour pressure. Assessment of the causes of these climate changes, however, is not within the scope of this paper. The results of future modelled evaporation are then discussed, followed by a discussion on changes in-lake temperature.

The modelled results under climate change are presented in an ensemble projection of the nine models used in this study, allowing for an assessment of the uncertainties implicit in the choice of the GCMs. The results are represented by the average of the outcomes from the nine climate models and the variability is indicated by the range between the 10th and the 90th percentile values, following similar studies (e.g., CSIRO and BoM, 2007 and Smith and Chandler, 2010).

5.2.1. Driving forces of evaporation under climate change

The 20-year average seasonal air temperature, wind speed, solar radiation and air vapour pressure projected for the periods

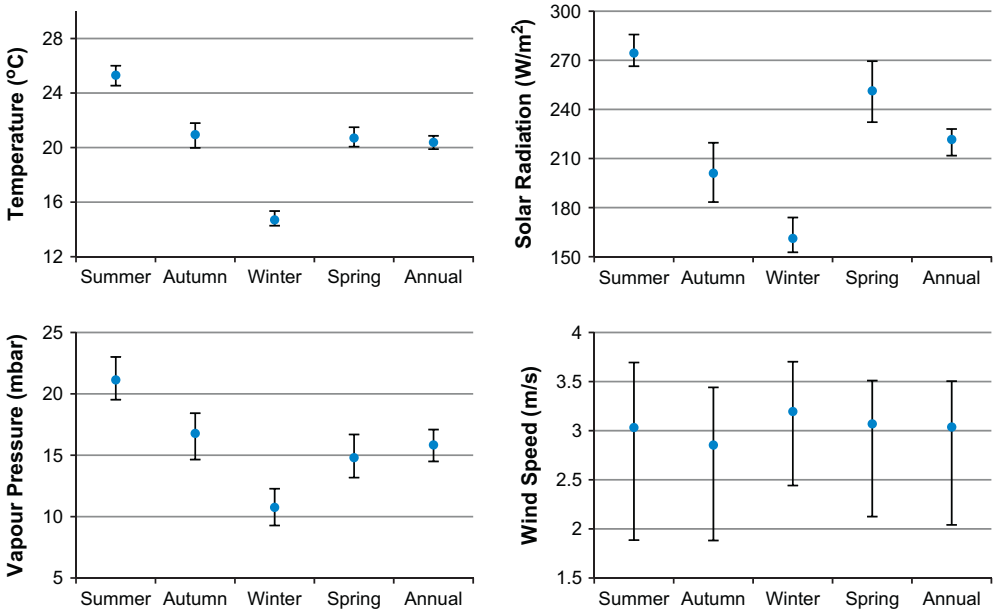

Fig. 3. 20-year average seasonal air temperature, solar radiation, vapour pressure and wind speed at Wivenhoe Dam. The whiskers represent the year-to-year variability and range from the 10th to the 90th percentiles. For the southern hemisphere, Summer = December, January and February; Autumn = March, April and May; Winter = June, July and August; Spring = September, October, November.

2030–2050 and 2070–2090 are summarized in Fig. 7. The red and green series represent the mean of the 20-year averages derived from the nine models, and the whiskers illustrate the intervals between the 10th and the 90th percentiles of the outcomes. The blue circles show the 20-year average values observed in the present-day scenario (1991–2010).

The data presented in Fig. 7 shows a slight increase of average annual surface air temperature in the period of 2030–2050 in relation to the present-day average climate. This increase is predicted to be approximately 1 °C, ranging between 0.8 °C and 1.3 °C, depending on the climate model. The most prominent rise in temperature for this period occurs in spring, when air temperatures are likely to increase by around 2 °C, representing a rise of 10% in relation to the present climate temperatures. The least significant rise is in autumn, when the average air temperature is expected to rise by an average of 0.7%. For 2070–2090, again all the models agree with a growth of the average air temperature in all seasons at the Wivenhoe Dam area. However, the estimated air temperature increases for this timeframe are more significant than the increases estimated for 2030–2050, lying between 1.7 and 3.2 °C (average of models = 2.7 °C). Higher air temperature increases are expected in spring and winter, with a rise ranging between 3 and 4 °C depending on the model. This represents an increase of approximately 20% in comparison with the baseline scenario air temperatures.

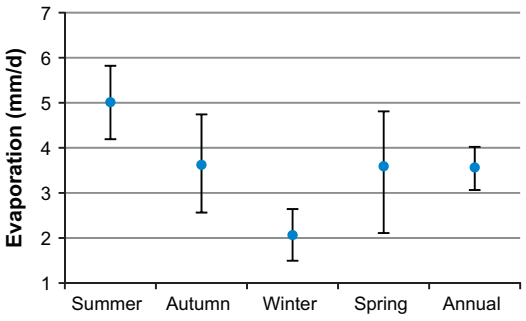

Fig. 4. Modelled seasonal daily evaporation from Wivenhoe Dam (averages of 20 recent years). The whiskers represent the year-to-year variability and range from the 10th to the 90th percentiles.

The average annual solar radiation is not expected to change significantly in 2030–2050 and 2070–2090 in relation to the present-day scenario. There is a slight rise in radiation for both timeframes, of around 0.5%. However, the estimated changes vary from −0.8% to 1.5% between the climate models, which makes it difficult to draw a definite conclusion about future annual solar radiation. However, seasonal changes in solar radiation are evident in both timeframes, as shown in the bar graphs in Fig. 7. Solar radiation is likely to go down in summer and autumn, but go up in winter and spring, in comparison to the baseline solar radiation. For 2030–2050, the range of change between models' results for spring and winter solar radiation is between 3% and 7% (average of models = 5%). For 2070–2080, this range is between 6% and 12%, with an average of 8% for both seasons. The decline in solar radiation in summer and autumn for the 2030–2050 timeframe is likely to be −2% and −5%, respectively. When looking at the 2070–2090 timeframe, the decrease in summer solar radiation is expected to be −4% and in autumn solar radiation, −11%.

According to the nine climate change models, future air vapour pressure is anticipated to be just slightly higher than the current long-term vapour pressure in all seasons and in both timeframes. The average increase in vapour pressure is approximately 0.5% in 2030–2050 and 1.2% in 2070–2090, with a range of change between models varying from −0.4% to 2% in 2030–2050 and from −0.9% to 4% in 2070–2090. An increase in average vapour pressure is expected in summer, winter and spring, for both periods of time. In summer, this growth is expected to be of around 1% and 1.4%, respectively for 2030–2050 and 2070–2090. In spring, it is expected to be slightly higher than in summer, at 1.2% and 3.2% for both timeframes respectively. In winter, the increase is in the order of only 0.3% for both time periods. As opposed to the other seasons, in autumn, vapour pressure will experience a small decrease, in the order of 0.3% in both timeframes.

The long-term average wind speed in the future projections is estimated to be just slightly lower than the long-term average wind speed observed in the present-day scenario. For 2030–2050, the average annual wind speed is projected to drop 1.6%.

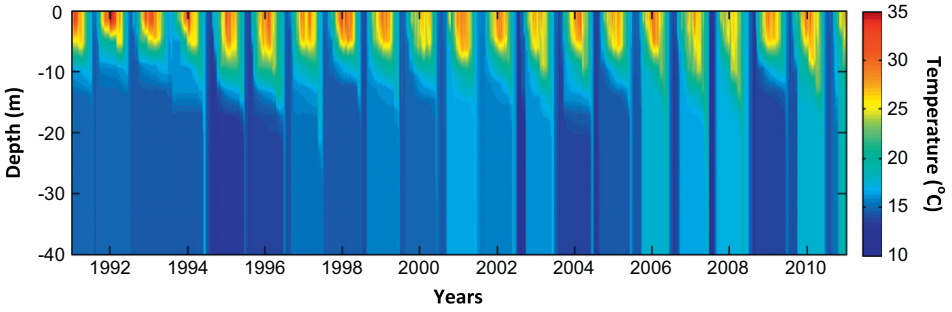

Fig. 5. Simulated water temperatures for Wivenhoe Dam – 01/01/1991 to 31/12/2010.

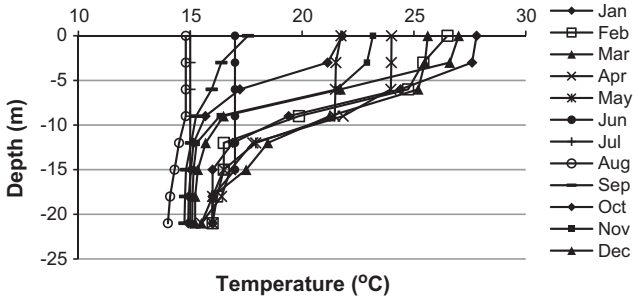

Fig. 6. Measured in-lake temperature profiles during the year of 2007 in Wivenhoe Dam. Available measurements were up to 21 m under the water.

For 2070–2090, it is likely to be 1.3% lower than today's wind speed. As for seasonality, no pronounced changes in wind speed are estimated in future summers. Wind magnitude is expected to slightly increase in spring, with the average growth from the nine models being 0.5% and 4.4% for the timeframes of 2030–2050 and 2070–2090, respectively. As opposed to spring and summer, considerable reductions in wind speed are expected in winter, with drops in the order of −5.2% and −8.6% for 2030–2050 and 2070–2090, respectively. Wind speed is also estimated to drop in future autumns. In the time period of 2030–2050, the expected decrease is approximately −1.5%, and in 2070–2090, −3.4%.

Fig. 8 shows the inter-model variability for the annual projections of air temperature, solar radiation, vapour pressure and wind speed. The red solid line represents the current 20-year annual average values. The grey bars show the 20-year average of the modelling data and the whiskers range between the 10th and the 90th percentiles. It can be seen that all the models predict a rise in air temperatures and that this rise is higher in the 2070–2090 timeframe. As for solar radiation, eight models predict an increase in solar radiation, but this increase is just slight for both timeframes. Similarly, average annual vapour pressure is also predicted by eight models to increase slightly. This increase is more significant in the 2070–2090 timeframe. The average annual wind speed is predicted by six models to be slightly less than the current 20-year average.

5.2.2. Evaporation under climate change

As a result of the aforementioned changes in climate, evaporation from Wivenhoe Dam is also expected to change, as is illustrated in Fig. 9.

Compared to the baseline evaporation, the average annual evaporation in the period 2030–2050 is likely to be 5.6% higher, and in the period of 2070–2090, 14.5% higher. In 2030–2050, annual evaporation is estimated to be 1400 mm, compared to the long-term annual evaporation in the present-day scenario of 1300 mm. It is important to note that all nine simulations predict higher evaporation rates than the current long-term average, as shown in Fig. 10. The variation in long-term annual evaporation for the 2030–2050 period ranges from 1330 mm to 1410 mm between the models. When looking at the 2070–2090 period of simulation, the average annual evaporation is 1490 mm, with variation between the models ranging from 1410 mm to 1540 mm. These increases are in accordance with the findings of Johnson and Sharma (2010), which also showed increase in average evaporation in Australia in 2030, 2050 and 2070 under the SRES-A2 scenario. They used outputs of five GCMs and the Penman equation to predict future evaporation rates over Australia.

Evaporation is expected to increase in summer, winter and spring in the future scenarios, with this rise being more pronounced in 2070–2090 than in 2030–2050. The more significant increases in evaporation are expected in spring, with an average increase of 21% in 2030–2050 and of 40% in 2070–2090. It is important to note that all considered models, with no exception, predict a significant rise in spring evaporation. The models' predictions vary between 13% and 26% for the 2030–2050 timeframe, and between 30% and 48% for 2070–2090. The main reasons behind the increase in spring evaporation – based on the expected changes in the climatic variables presented in Fig. 7 – are the significant increases in surface air temperatures, which are likely to rise by around 2 °C in 2030–2050 and by 4 °C in 2070–2090, solar radiation and the slight increases in wind speed.

In winter, evaporation is expected to increase by 1% in 2030–2050 and by 14% in 2070–2080. In the 2030–2050 timeframe, the results using the nine climate models showed an inter-variation ranging from -2% to 4%. Therefore, some of the models predict a decrease in winter evaporation, which can be attributed to the significant reductions in wind speed. These reductions may outweigh the effects of increasing air temperatures and solar radiation during this season. Nevertheless, most of the models predict a rise in winter evaporation, resulting in an average increase of 1% in relation to the baseline scenario. In the 2070–2090 timeframe, on the other hand, all models predict higher evaporation rates in winter, varying from 9% to 21% above the baseline values. The main cause of these increases is the significant elevation in air temperatures in winter. Even with lower wind speeds, winter evaporation in 2070–2090 is still greater than winter evaporation in the control scenario due to the higher air temperatures.

In summer, evaporation is expected to increase by 5% in 2030–2050 and by 12% in 2070–2090. Increased summer evaporation is estimated by all of the models, and the main cause of this rise is the elevation in air temperatures. Even with predicted decreases in wind speed and solar radiation, and slight increases in vapour pressure, the resulting effect is still an increase in evaporation in summer, attributable to the higher air temperatures.

Autumn is the only season when evaporation is predicted to be lower than the current long-term evaporation. The reduction is predicted to be, on average, −5.5% in 2030–2050 and −8% in

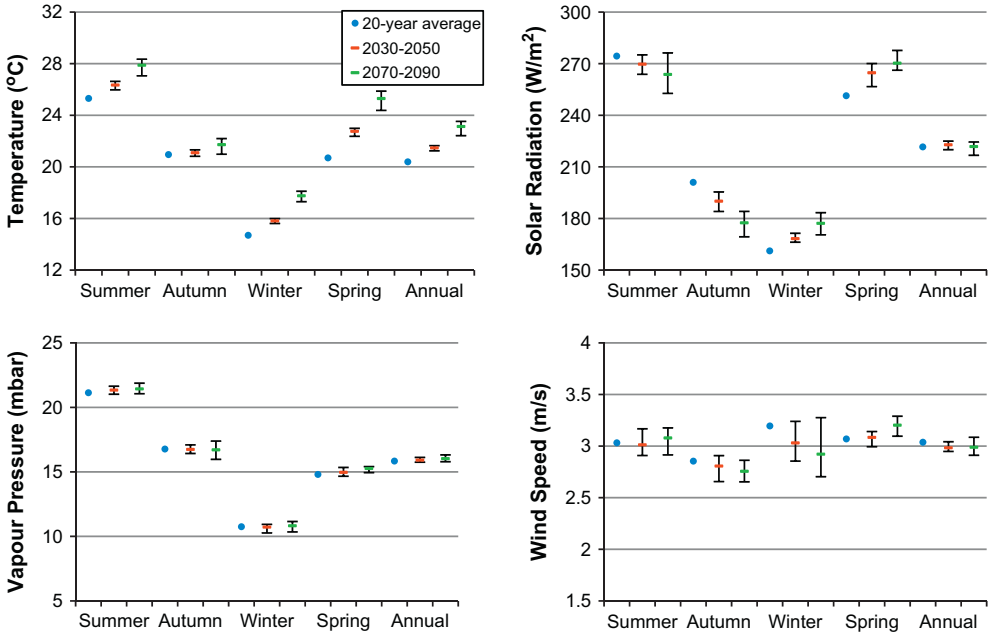

Fig. 7. Current and future seasonal air temperature, solar radiation, vapour pressure and wind speed at Wivenhoe Dam. The red and green series represent the mean of the 20-year average values derived from the nine models, and the whiskers illustrate the intervals between the 10th and the 90th percentiles of the models' outcomes. The blue circles show the 20-year average values observed in the present-day scenario (1991–2010).

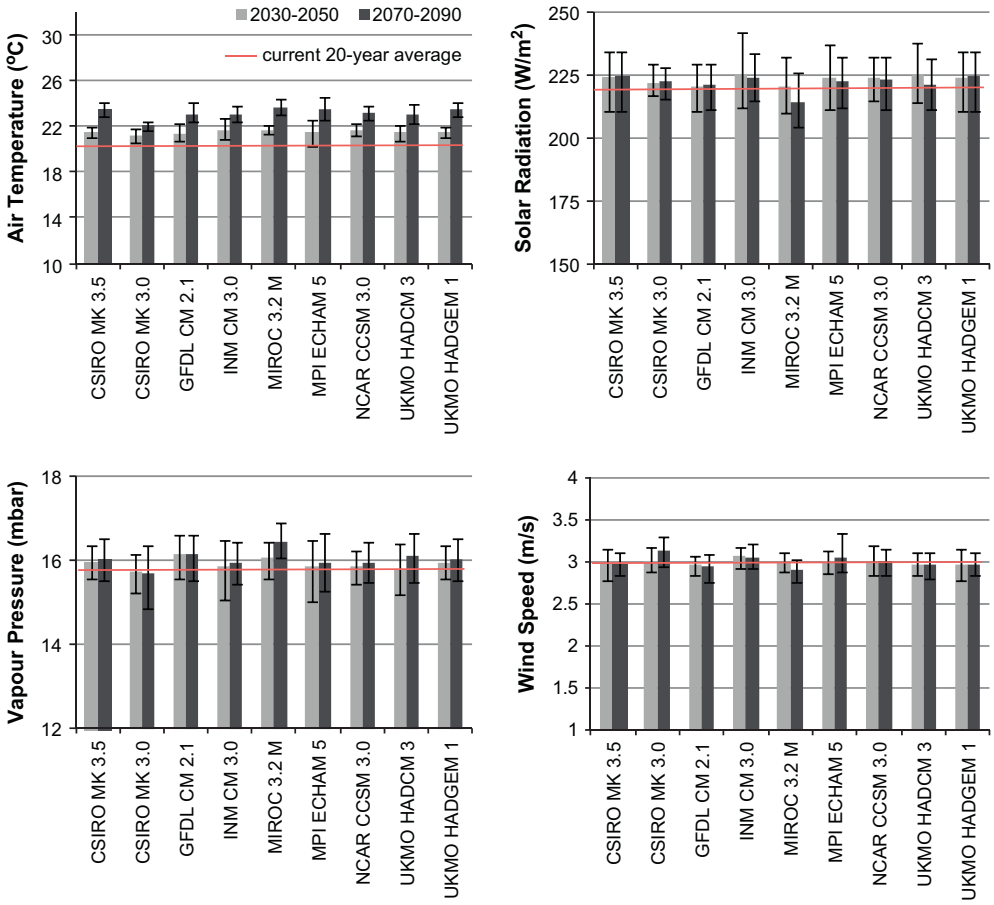

Fig. 8. Current and future annual air temperature, solar radiation, vapour pressure and wind speed at Wivenhoe Dam (averages of 20 years). The red solid line shows the observed 20-year average values in the present-day scenario (1991–2010). The grey bars show the average of 20 years of modelling predictions. The whiskers illustrate the year to year variability and range between the 10th and the 90th percentiles of the models' outcomes.

2070–2090. All the models adopted in this study resulted in lowering of evaporation rates in autumn. The variation between the models is between −2.7% and −9% in the 2030–2050 timeframe, and between −3.5% and −12% in the 2070–2090 timeframe. The main factors leading to reduced evaporation rates in this season are the reductions in solar radiation and wind speed. The effects from these reductions on evaporation outweighed the effects of the slight increases in air temperatures, as shown in Fig. 7.

Fig. 11 shows the predictions after weighting the evaporation results from the nine models based on the *M* score for each model. This score, as mentioned earlier, is based on the agreement between simulated and observed seasonal-mean air temperatures, precipitation and sea level pressure across Australia. Even though this score is not based on evaporation projections, it is still one of the closest available forms of assessing the quality of the projections. Models with higher *M* value were assumed to give more reliable projections of future climate, and therefore were assigned a higher weight (e.g., 27% for ECHAM5, and 21% for CCSM3, which predict the current average climate with higher level of accuracy in comparison with the other models).

As noted in Figs. 11 and 9, the results with the model weighting system did not differ from the results obtained without a weighting system. According to both methods, higher evaporation rates are expected in future summers and springs and lower evaporation in future autumns. In winter, evaporation is only significantly higher than the baseline values in the 2070–2090 timeframe. Both methods also yielded similar magnitudes for the future annual evaporation rates.

5.2.3. Lake temperature under climate change

The changes in climate presented in Fig. 7 also affect Wivenhoe Dam temperatures, as shown in Fig. 12. Overall, it can be seen that there is an increase in the long-term average surface temperature of Wivenhoe Dam in the future scenarios in comparison to the baseline long-term average lake surface temperature. The average lake surface temperature increases from 22.4 °C (baseline value) to 23.1 °C in 2030–2050, and to 24.05 °C in 2070–2090. All of the models predict an increase in the average lake surface temperature (Fig. 13). In 2030–2050, the variation between the outcomes from the nine models lies between 0.55 °C and 0.80 °C, whereas in 2070–2090, it lies between 1 °C and 2 °C.

Lake surface temperatures are expected to increase more significantly in spring. For the 2030–2050 timeframe, the increase is expected to be 1.7 °C in relation to the baseline spring lake surface temperatures. For the 2070–2090 timeframe, the increase is even higher, at 3.3 °C in comparison to today's spring lake temperatures. Also significant are the changes expected in winter. In this season, lake surface temperatures in 2030–2050 are estimated to be 1 °C higher than the baseline winter surface temperatures, and 2.5 °C higher in 2070–2090. In summer there is also a predicted increase in-lake surface temperatures, but this is not as pronounced as the increases estimated for winter and spring. The increase in summer lake surface temperatures is expected to be 0.4 °C in 2030–2050 and 1 °C in 2070–2090 in comparison to the baseline lake temperatures in summer.

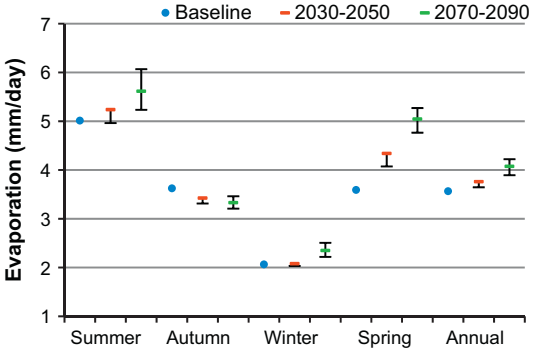

Fig. 9. Modelled current and future seasonal evaporation from Wivenhoe Dam (averages of 20 years). The blue circles show the 20-year average modelled results obtained using observed data from 1991 to 2010.The red and green series represent the average of modelled results using climate change models' predictions. The whiskers show the interval between the 10th and 90th percentiles of the averages of the nine models' outcomes. (For interpretation of the references to colour in this figure legend, the reader is referred to the web version of this article.)

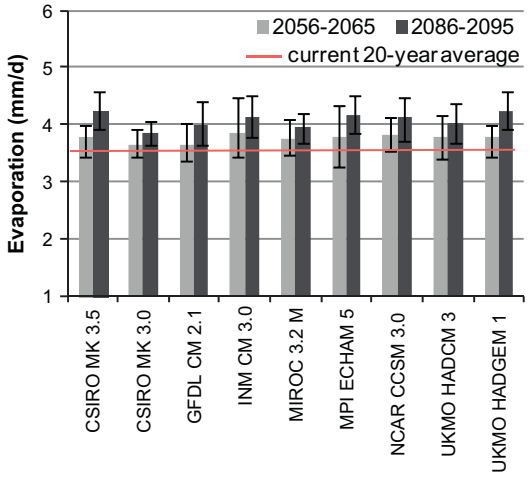

Fig. 10. Modelled current and future annual average daily evaporation from Wivenhoe Dam (averages of 20 years). The red solid line shows the modelled 20-year average values obtained with observed meteorological variables from 1991 to 2010. The grey bars show the modelled 20-year average results obtained using climate change models' predictions. The whiskers illustrate the year to year variability and range between the 10th and the 90th percentiles of the models' outcomes.

The volume-averaged temperature of Wivenhoe Dam is estimated to be approximately 19 °C in the present-day scenario. The simulations with the future climate projections resulted in an average lake temperature of 19.5 °C in 2030–2050 and 20.5 °C in 2070–2090. As with lake surface temperature, the average lake temperature is also expected to increase more significantly in spring than in the other seasons. The higher water temperatures in spring explain the more pronounced increase in evaporation in this season.

Table 2 summarizes the changes predicted in the meteorological variables used in the modelling of evaporation, as well as the changes in-lake temperature and in evaporation from Wivenhoe Dam for the two future timeframes adopted in this study (2030–2050 and 2070–2090). The changes are categorised as significant, slight and unchanged. The table shows that the main agents behind the significant increases in evaporation and lake temperature in the future timeframes (e.g., in spring) are primarily the increased surface air temperatures. Ii is also noticeable that wind speed plays an important role in the determination of evaporation rates. Even small increases/decreases in this climatic variable will cause a significant change in evaporation. For instance, in 2030–2050, the models predict a significant increase in air temperature and a slight increase in solar radiation in both winter and spring seasons. In winter, however, there is a slight reduction in wind speed, whereas in spring, there is no change in wind speed. The slight reduction in wind speed in winter counterbalanced the increases in air temperature and solar radiation, resulting in unchanged evaporation rates in this season. In spring, however, as there was no change in wind speed and therefore, nothing to counterbalance the high air temperatures and solar radiation, the result was a significant increase in evaporation. This important effect of the wind can

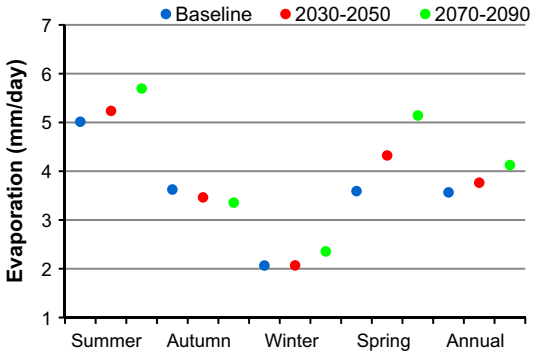

Fig. 11. Modelled current and future seasonal evaporation from Wivenhoe Dam (averages of 20 years) using a model weighting system.

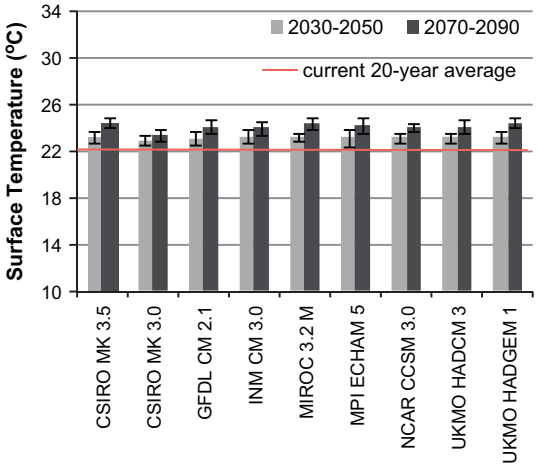

Fig. 13. Modelled current and future annual average surface temperature of Wivenhoe Dam (averages of 20 years). The red solid line shows the modelled 20-year average values obtained with observed meteorological variables from 1991 to 2010. The grey bars show the modelled 20-year average results obtained using climate change models' predictions. The whiskers illustrate the year to year variability and range between the 10th and the 90th percentiles of the models' outcomes.

be explained by the aerodynamic model used to estimate evaporation in the model DYRESM. This model is largely sensitive to changes in this parameter.

Fig. 14 shows the average volume-averaged lake water temperature from 1991 to 2010 and for the two future projections. There is a noticeably gradual increase of warming of Wivenhoe Dam over the years. From 1991 to 2010, the rate of warming was 0.02 °C per year. From 2030 to 2050, the warming rate is estimated to be approximately 0.03 °C per year. From 2070 to 2090, the rate of warming is likely to reach 0.035 °C per year. The impact of such changes will not only affect evaporation rates, but also the biological activity of the lake. For instance, higher water temperatures will decrease the maximum amount of oxygen that can be dissolved in the water, leading to oxygen stress if the water receives high loads of organic matter. This will have a negative impact on the biological processes of fish including growth, reproduction and behaviour.

6. Conclusions

This study analysed the changes in water temperatures and evaporation from a large Australian reservoir under climate change conditions using modelling. The conclusions drawn here are based on Wivenhoe Dam, a temperate lake located in the state of Queensland.

The climate change scenario used in this study was the SRES-A2 emission scenario, which is a realistic scenario based on current global greenhouse gas emissions. Two future timeframes were used, one from 2030 to 2050 and the other from 2070 to 2090. Projected daily meteorological data from nine global climate models downscaled to a 15-km resolution grid over the study area were used to derive daily water column temperatures and evaporation rates through modelling with the well-established 1-D model DYRESM. The projected modelled water temperatures and evaporation rates were compared to modelled water temperatures and evaporation rates obtained with observed meteorological data from the period of 1991 to 2010. An ensemble of projections was used in this assessment to account for the uncertainties involved in the choice of climate models.

The simulations showed that the long-term average annual evaporation from Wivenhoe Dam is 1,300 mm. While the average annual evaporation in 2030–2050 is slightly higher than the baseline evaporation, at 1400 mm, and the predicted average annual evaporation in 2070–2090 is considerably higher, at 1490 mm. This is in agreement with the work of Johnson and Sharma (2010), who has also demonstrated that evaporation will increase in Australia in the future.

By observing the future climate against the evaporation predictions, it can be concluded that the main changes in the driving forces that bring about the increase in evaporation are the increased surface air temperatures. Higher air temperatures are expected in the future in all four seasons, particularly in summer, winter and spring, while higher wind speeds are expected in summer, autumn and spring.

The season which will experience higher changes in evaporation is spring, due to not only higher air temperatures, but also

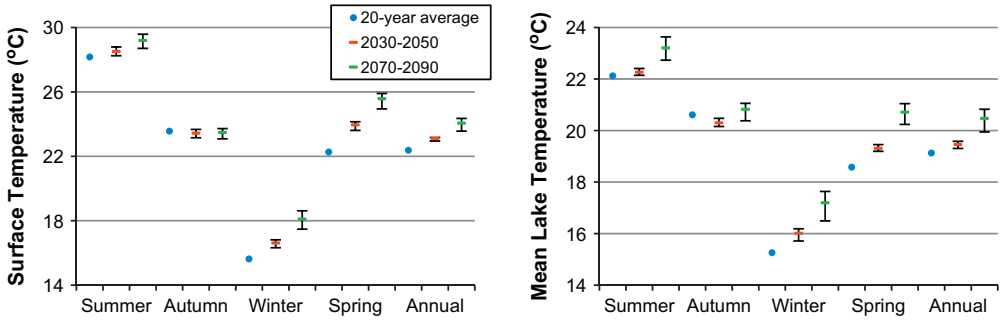

Fig. 12. Modelled current and future seasonal temperatures of Wivenhoe Dam (averages of 20 years). The blue circles show the 20-year average modelled results obtained using observed data from 1991 to 2010.The red and green series represent the average of modelled results using climate change models' predictions. The whiskers show the interval between the 10th and 90th percentiles of the averages of the nine models' outcomes.

Table 2
Significance of the future changes in meteorological variables (air temperature, solar radiation, vapour pressure and wind speed), lake temperature and evaporation from Wivenhoe Dam.

	Summer	Autumn	Winter	Spring	Annual
2030–2050					
Air temperature[a]	Significant increase	No change	Significant increase	Significant increase	Significant increase
Solar radiation[b]	Slight decrease	Slight decrease	Slight increase	Slight increase	No change
Vapour pressure[b]	No change	No change	No change	Slight increase	No change
Wind speed[b]	No change	Slight decrease	Slight decrease	No change	Slight decrease
Lake temperature[a]	No change	No change	Significant increase	Significant increase	Slight increase
Evaporation[c]	Slight increase	Slight decrease	No change	Significant increase	Slight increase
2070–2090					
Air temperature[a]	Significant increase	Slight increase	Significant increase	Significant increase	Significant increase
Solar radiation[b]	Slight decrease	Significant decrease	Significant increase	Significant increase	No change
Vapour Pressure[b]	Slight increase	No change	No change	Slight increase	Slight increase
Wind speed[b]	Slight increase	Slight decrease	Significant decrease	Slight increase	Slight decrease
Lake temperature[a]	Significant increase	No change	Significant increase	Significant increase	Significant increase
Evaporation[c]	Slight increase	Slight decrease	Slight increase	Significant increase	Significant increase

[a] Significant: >1 °C change/slight: 0.5–1 °C change/no change: <0.5 °C change.
[b] Significant: >6% change/slight: 1–6% change/no change: <1% change.
[c] Significant: >15% change/slight: 4–15% change/no change: <3% change.

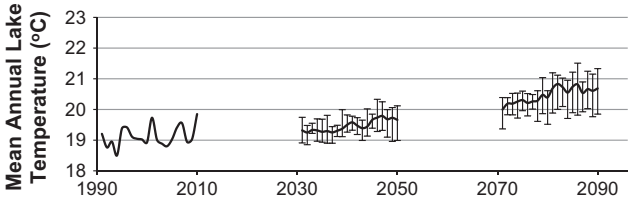

Fig. 14. Mean temperature of Wivenhoe Dam in current (1991–2010) and future scenarios – modelled results. The whiskers extend from the 10th to 90th percentiles of the results from the nine models used in the simulations.

higher solar radiation and wind speeds. As opposed to spring, autumn seasons will experience a slight decrease in evaporation, due to decrease in solar radiation and wind speeds.

Therefore, it appears that evaporation from SEQ reservoirs will increase in the future, but this increase will not be significantly higher than the baseline evaporation over the next 50 years. Beyond this timeframe however, important increases in evaporation are expected, particularly in the warm seasons (summer and spring). It is important to note that the seasonal distribution of precipitation has shown by the models to slightly change in the future scenarios as compared to the baseline distribution, with increases in precipitation in summer and decreases in evaporation in the other seasons under climate change scenarios. Total annual precipitation, however, is predicted not to change in the SEQ region. This demonstrates that with a growing economy and population, and considering that annual rainfall will remain unchanged, SEQ will have to either increase water availability through construction of additional reservoirs or desalination plants, or decrease the losses of water through, for instance, the employment of technologies to reduce evaporation from the existing reservoirs.

As a result of a changing climate, particularly higher surface air temperatures, lake temperature will also be different. The average volume-average temperature of Wivenhoe Dam is likely to change from 19 °C in the baseline scenario to 19.5 °C and 20.5 °C in the periods of 2030–2050 and 2070–2090 respectively. The changes in-lake temperature are more pronounced in winter and spring than in the other seasons in 2030–2050. For 2070–2090, significant lake warming is expected in summer, winter and spring. The results also showed that Wivenhoe Dam has been warming over the past decades and will warm at even higher rates towards the end of the century.

In regard to the research methodology, the results of this study were derived from thermodynamic modelling of Wivenhoe Dam using forcings obtained from nine GCMs downscaled over the SEQ region. The nine GCMs were selected by the CSIRO, Australia, from the 23 available GCMs, based on their efficacy in simulating the control climate of SEQ. The results of the simulations from this study were presented and assessed in an ensemble projection of the nine models in order to account for the uncertainties implicit in the choice of the GCMs. Hence, the results were shown as a range of probable outcomes or, more precisely, as an envelope of projections forced by the nine GCMs. This multi-model approach has been found to provide better forecasts than single-model approaches, in terms of skill, reliability and consistency, particularly when considering many variables or diagnostics (Johnson and Sharma, 2009). Attempts to reduce the biases in future projections should never be made by removing models arbitrarily from an analysis. Although the current approach recognises the impossibility of obtaining an exact magnitude for future evaporation and temperature changes of Wivenhoe Dam, it at least provides an initial insight into the relevant trends, as well as into what is most likely to happen in the future.

The approach of this study has international applicability as the method used to estimate evaporation differs from the traditional methods, mostly based on the Penman model. The method in this study takes into account the temporal and spatial changes in-lake water temperature, driven by meteorological boundary conditions derived from the downscaled climate change projections. This method is generic and can be applied to different regions and not just to the case presented here. Moreover, we recommend that studies like this should be incorporated in local long-term integrated water resources management plans to account for the probable changes in water availability. This will then assist in sound decision-making concerning water resources management and planning. The adoption of this methodology to other reservoirs in Australia in order to determine a national trend is what we recommend for further investigation.

Acknowledgments

We acknowledge the modelling groups, the Program for Climate Model Diagnosis and Intercomparison (PCMDI), and the WCRP's Working Group on Coupled Modelling (WGCM) for their roles in making available the WCRP CMIP3 multi-model dataset. Support of this dataset is provided by the Office of Science, U.S. Department of Energy. We also thank the CSIRO and the Bureau of Meteorology

for making available the downscaled data from the nine models utilised in this study.

Funding for this project was provided by Griffith Climate Change Response Program, Griffith University Postgraduate Research School through the GUPRS scholarship, the Australian Government Department of Innovation, Industry, Science and Research through the IPRS scholarship, the Griffith School of Engineering and the Urban Water Research Security Alliance.

References

Brutsaert, W., 1982. Evaporation into the Atmosphere. Reidel, Dordrecht, 299 p.
Charles, S.P., Bari, M.A., Kitsios, A., Bates, B.C., 2007. Effect of GCM bias on downscaled precipitation and runoff projections for the Serpentine catchment, Western Australia. Int. J. Climatol. 27 (12), 1673–1690.
Chu, J.T., Xia, J., Xu, C., Singh, V.P., 2010. Statistical downscaling of daily mean temperature, pan evaporation and precipitation for climate change scenarios in Haihe River, China. Theor. Appl. Climatol. (1–2), 149–161.
Collins, W.D. et al., 2006. The community climate system model version 3 (CCSM3). J. Climate 19 (11), 2122–2143.
Craig, I., Green, A., Scobie, M., Schmidt, E., 2005. Controlling Evaporation Loss from Water Storages. Report 1000580/1, National Centre for Engineering in Agriculture, Toowoomba, 207 p.
CSIRO and BOM, 2007. Climate Change in Australia. Technical Report of CSIRO, Bureau of Meteorology and the Australian Greenhouse Office in Partnership with the Australian Climate Change Science Program, Canberra, 148 p.
Delworth, T.L. et al., 2006. GFDL's CM2 global coupled climate models. Part I: Formulation and simulation characteristics. J. Climate 19 (5), 643–674.
Diansky, N.A., Volodin, E.M., 2002. Simulation of present-day climate with a coupled atmosphere-ocean general circulation model. (Engl. Transl.). Izv. Atmos. Ocean. Phys. 38 (6), 732–747.
Gordon, C. et al., 2000. The simulation of SST, sea ice extents and ocean heat transports in a version of the Hadley Centre coupled model without flux adjustments. Climate Dyn. 16, 147–168.
Gordon, H.B., et al., 2010. The CSIRO Mk3.5 Climate Model. Technical Report no. 021, Centre for Australian Weather and Climate Research (A Partnership between CSIRO and the Bureau of Meteorology), Melbourne, 62 p.
Gordon, H.B., et al., 2002. The CSIRO Mk3 Climate System Model. Technical Paper 60, CSIRO Atmospheric Research, Melbourne, 130 p.
Haerter, J.O., Hagemann, S., Moseley, C., Piani, C., 2011. Climate model bias correction and the role of timescales. Hydrol. Earth Syst. Sci. 15, 1065–1079.
Hasumi, H., et al., 2004. K-1 Coupled GCM (MIROC) Description. Technical Report No. 1 of the K-1 model developers. Centre for Climate System Research, University of Tokyo, Tokyo, 34 p.
Hay, L.E., Wilby, R.L., Leavesley, G.H., 2000. A comparison of delta change and downscaled GCM scenarios for three mountainous basins in the United States. J. Am. Water Resour. As. 36, 387–397.
Helfer, F., Zhang, H., Lemckert, C., 2011. Modelling of lake mixing induced by air-bubble plumes and the effects on evaporation. J. Hydrol. 406, 182–198.
Hocking, G.C., Sherman, B.S., Patterson, J.C., 1988. Algorithm for selective withdrawal from stratified reservoir. J. Hydraul. Div. ASCE 114, 707–719.
Imberger, J., Patterson, J.C., 1981. A dynamic reservoir simulation model – DYRESM. In: Fischer, H.B. (Ed.), Transport Models for Inland and Coastal Waters. Academic Press, New York, pp. 310–361.
Imberger, J., Patterson, J.C., Hebbert, B., Loh, I., 1978. Dynamics of reservoir of medium size. J. Hydraul. Div. ASCE 104 (HY5), 725–743.
IPCC, 2000. Special Report on Emissions Scenarios (SRES). Special Report of Working Group III of the Intergovernmental Panel on Climate Change. Cambridge University Press, Cambridge, 570 p.
IPCC, 2007. Climate Change 2007: The Physical Science. Contribution of Working Group I to The Fourth Assessment Report of the IPCC (AR4). Cambridge University Press, Cambridge, 996 p.
Ivey, G.N., Patterson, J.C., 1984. A model of the vertical mixing in Lake Erie in summer. Limnol. Oceanogr. 29, 553–563.
Johns, T.C. et al., 2006. The new Hadley Centre climate model HadGEM1: evaluation of coupled simulations. J. Climate 19 (7), 1327–1353.
Johnson, F., Sharma, A., 2009. Measurement of GCM skills in predicting variables relevant for hydroclimatological assessments. J. Climate 22, 4373–4382.
Johnson, F., Sharma, A., 2010. A comparison of Australian open water body evaporation trends for current and future climates estimated from class a evaporation pans and general circulation models. J. Hydrometeor. 11, 105–121.
Kay, A.L., Davies, H.N., 2008. Calculating potential evaporation from climate model data: a source of uncertainty for hydrological climate change impacts. J. Hydrol. 358 (3–4), 221–239.
Kay, A.L., Jones, R.G., Reynard, N.S., 2006. RCM rainfall for UK flood frequency estimation. II. Climate change results. J. Hydrol. 318 (1–4), 163–172.
Kirono, D.G.C., Kent, D.M., 2011. Assessment of rainfall and potential evaporation from global climate models and its implications for Australian regional drought projection. Int. J. Climatol. 31, 1295–1308.
Leander, R., Buishand, T.A., van den Hurk, B.J.J.M., de Wit, M.J.M., 2008. Estimated changes in flood quantiles of the river Meuse from resampling of regional climate model output. J. Hydrol. 351 (3–4), 331–343.
Lenderink, G., Buishand, A., van Deursen, W., 2007. Estimates of future discharges of the river Rhine using two scenario methodologies: direct versus delta approach. Hydrol. Earth Syst. Sci. 11, 1145–1159.
Martin, G.M. et al., 2006. The physical properties of the atmosphere in the new Hadley Centre Global Environmental Model, HadGEM1. Part 1: Model description and global climatology. J. Climate 19 (7), 1274–1301.
McGregor, J.L., 2005. C-CAM: Geometric Aspects and Dynamical Formulation. CSIRO Atmospheric Research Technical Paper no. 70, 43 p.
McGregor, J.L., Dix, M.R., 2001. The CSIRO Conformal-cubic Atmospheric GCM. In: Proceedings of the IUTAN Symposium on Advances in Mathematical Modelling of Atmospheric and Ocean Dynamics, July 02–07, 2000, Dordrecht, pp. 197–202.
McGregor, J.L., Dix, M.R., 2008. An updated description of the Conformal-Cubic Atmospheric Model. In: Hamilton, K., Ohfuchi, W. (Eds.), High Resolution Numerical Modelling of the Atmosphere and Ocean. Springer, pp. 51–76.
McGregor, J.L., Nguyen, K., 2010. Dynamical Downscaling from Climate Change Experiments. Final Report for Project 2.1.5b, CSIRO Land and Water, 21 p.
Meehl, G.A. et al., 2007. The WCRP CMIP3 multimodel dataset: a new era in climate change research. Bull. Am. Meteorol. Soc. 88 (9), 1383–1394.
Nguyen, K., Katzfey, J., McGregor, J., 2011. Global 60 km simulations with CCAM: evaluation over the tropics. Clim. Dynam., pp. 1–18, (accepted, doi 10.1007/s00382-011-1197-8).
Nunez, M., McGregor, J.L., 2007. Modelling future water environments of Tasmania, Australia. Climate Research: Interactions of Climate with Organisms, Ecosystems, and Human Societies 34, 25–37.
Patterson, J.C., Hamblin, P.F., Imberger, J., 1984. Classification and dynamic simulation of the vertical density structure of lakes. Limnol. Oceanogr. 29 (4), 845–861.
Patterson, J.C., Imberger, J., 1989. Simulation of bubble plume destratification systems in reservoirs. Aquat. Sci. 51, 3–18.
Perkins, S.E., Pitman, A.J., Holbrook, N.J., McAneney, J., 2007. Evaluation of the AR4 climate models simulated daily maximum temperature, minimum temperature, and precipitation over Australia using probability density functions. J. Climate 20, 4356–4376.
Pope, V., Gallani, M.L., Rowntree, P.R., Stratton, R.A., 2000. The impact of new physical parameterizations in the Hadley Centre climate model: HadAM3. Clim. Dynam. 16, 123–146.
Raupach, M.R. et al., 2007. Global and regional drivers of accelerating CO_2 emissions. Proc. Nat. Acad. Sci. 104, 10288–10293.
Ringer, M.A. et al., 2006. The physical properties of the atmosphere in the new Hadley Centre Global Environmental Model, HadGEM1. Part 2: Aspects of variability and regional climate. J. Climate 19 (7), 1302–1326.
Roeckner, E., et al., 2003. The Atmospheric General Circulation Model ECHAM5. Part I: Model Description. MPI Report no. 349. Max Planck Institute for Meteorology, Hamburg, 127 p.
Sahoo, G.B., Schladow, S.G., 2008. Impacts of climate change on lakes and reservoirs dynamics and restoration policies. Sustain. Sci. 3, 189–199.
Sherman, F.S., Imberger, J., Corcos, G.M., 1978. Turbulence and mixing in stably stratified waters. A. Rev. Fluid Mech. 10, 267–288.
Smith, I., Chandler, E., 2010. Refining rainfall projections for the Murray Darling Basin of south-east Australia – the effect of sampling model results based on performance. Climatic Change 102 (3), 377–393.
Spigel, R.H., Imberger, J., 1980. The classification of mixed-layer dynamics in lakes of small to medium size. J. Phys. Oceanogr. 10 (7), 1104–1121.
Thatcher, M., McGregor, J.L., 2011. A technique for dynamically downscaling daily-averaged GCM datasets using the Conformal Cubic Atmospheric Model. Mon. Weather Rev. 139, 79–95.
van Roosmalen, L., Christensen, J.H., Butts, M.B., Jensen, K.H., Refsgaard, J.C., 2010. An intercomparison of regional climate model data for hydrological impact studies in Denmark. J. Hydrol. 380, 406–419.
Watterson, I.G., 1996. Non-dimensional measures of climate model performance. Int. J. Climatol. 16, 379–391.
Xu, Y., Zong-Liang, Y., 2012. A Method to Study the Impact of Climate Change on Variability of River Flow: An Example from the Guadalupe River in Texas. Climatic Change 113 (3), 965–979.
Yao, X., 2008. An Improved 2-D Numeric Model for Open-water Daily Evaporation Estimation. BA of Science Thesis, Griffith University, Gold Coast, Australia, 59 p.
Yeates, P.S., Imberger, J., 2003. Pseudo two-dimensional simulations of internal and boundary fluxes in stratified lakes and reservoirs. Intl. J. River Basin Manage. 1 (4), 297–319.
Yilmaz, A.G., Imteaz, M.A., 2011. Impact of climate change on runoff in the upper part of the Euphrates basin. Hydrolog. Sci. J. 56 (7), 1265–1279.